HHS Public Access

Author manuscript

Wound Repair Regen. Author manuscript; available in PMC 2018 November 20.

Published in final edited form as:

Wound Repair Regen. 2017 May ; 25(3): 541–549. doi:10.1111/wrr.12527.

Histopathological comparisons of *Staphylococcus aureus* and *Pseudomonas aeruginosa* experimental infected porcine burn wounds

Sarah B. Chaney, DVM, Dipl. ACVP[1,3], **Kasturi Ganesh, MD**[2], **Shomita Mathew-Steiner, PhD**[2], **Paul Stromberg, PhD, DVM, Dipl. ACVP**[1], **Sashwati Roy, PhD**[2], **Chandan K. Sen, PhD**[2], and **Daniel J. Wozniak, PhD**[3]

[1]Department of Veterinary Bioscience, College of Veterinary Medicine, Columbus, Ohio

[2]Department of Surgery, Comprehensive Wound Center, Davis Heart and Lung Research Institute, Columbus, Ohio

[3]Department of Microbial Infection and Immunity, The Ohio State University, Columbus, Ohio

Abstract

Chronic skin wounds are a significant human health concern and are often complicated by infection with *Pseudomonas aeruginosa* and *Staphylococcus aureus*, particularly methicillin resistant *S. aureus* (MRSA). Translating the knowledge gained from extensive study of virulence mechanisms and pathogenesis of these bacterial species to new treatment modalities has been lacking in part due to a paucity of animal models able to recapitulate human disease. Our groups recently described a novel porcine chronic burn wound model for the study of bacterial infection; however, the histopathology of infection has yet to be described. The objective of this study is to define the histopathology of this model using important human chronic wound bacterial isolates. Porcine full-thickness burn wounds topically inoculated with *P. aeruginosa* strain PAO1, MRSA *S. aureus* strain USA300 or both bacteria were used to define and quantify histopathologic lesions. The development of a systemic, well-defined rubric for analysis allowed for evaluation of differences between infection groups. These differences, which included epithelial migration and proliferation, stromal necrosis, fluid accumulation and intensity and character of the innate and adaptive inflammatory cell responses, were identified temporally between infection groups. Mono-species infected wounds developed a hyper-proliferative wound edge. Coinfected wounds at day 35 had the largest wound sizes, increased amounts of neutrophilic inflammation, immaturity of the wound bed, and retention of necrotic tissue. Infection, regardless of species, inhibited wound contracture at all time points evaluated. Most importantly, this model recapitulated key features of chronic human wounds. Thus, this model will allow researchers to study novel treatment modalities in a biologically relevant animal model while monitoring both host and bacterial responses.

Reprint requests: Daniel J. Wozniak, 704 BRT, 460 West, 12th Avenue, Columbus, OH 43210., Tel: 614-247-7629 (Office), 614-688-1619 (Lab);, Fax: 614-292-9616;, daniel.wozniak@osumc.edu.

Conflicts of Interest: The authors have no financial conflicts that might pose or create a conflict of interest.

Supporting Information

Additional supporting information may be found in the online version of this article.

Chronic wounds are a major health care concern worldwide with millions of people affected each year and annual treatment expenditure estimated to be several billion dollars.[1] The increasing incidence of obesity, diabetes, nosocomial postoperative surgical infections, combat related wound infections, and growing elderly population make wound care a significant public health concern. Due to the multifactorial contributing factors and complexities of this microenvironment (i.e., ischemia, infection status, comorbidities, immune status), developing an all-encompassing model is not realistic. However, in an attempt to address and understand wound healing, numerous animal models of chronic wound healing have been developed (reviewed in Ganesh et al.[2]). Bacterial persistence is a significant contributor to delayed healing with an astounding 60% of all chronic wounds having a chronic bacterial infection. *Staphylococcus aureus* and *Pseudomonas aeruginosa* account for the most common human wound bacterial isolates regardless of the initiating cause of soft tissue injury.[3]

While the term *chronic wound* encompasses a broad range of disease and clinical presentations, the histopathology of human chronic wounds has some common microscopic features; the most detailed of which are a proliferative wound edge with hyperkeratosis and variably fibrotic wound bed with neutrophilic inflammation.[4] In contrast, the histopathology of animal models of chronic wounds are poorly characterized making drawing parallels between human and model systems difficult. Also, a lack of consistent criteria to evaluate host healing and response to infection makes comparison between animal models challenging and experimentation redundant. We aimed to detail the histopathology of the host response to various bacterial infections using common human bacterial isolates in our newly described animal model. The rubric developed here provides a means to evaluate future comparisons between treatment groups and infection types. Correlation to human pathology is also discussed.

MATERIALS AND METHODS

Animals

The Ohio State University's Institutional Laboratory Animal Case and Use Committee (protocol 2012A00000041-R1) approved all experiments. Female Yorkshire pigs weighing between 70 and 80 pounds were used in this study ($n = 11$).

Bacterial isolates

P. aeruginosa strain PAO1 was obtained from the Matthew Parsek Laboratory and a spontaneous rifampicin mutation was generated from overnight culture on tryptic soy agar (TSA) with 100 μg/mL rifampicin.[5] *S. aureus* strain USA300 was obtained from the Network on Antimicrobial Resistance in *S. aureus* (NARSA, BEI Resources Repository, NAID, NIH, Manassas, VA) and was grown on TSA plates or broth media.

Porcine burn wound model

Porcine infections were carried out as previously described.[6] In brief, reproducible, full-thickness burn wounds were established under general anesthesia on the paravertebral, dorsolateral trunk, bilaterally. A total of six, $2'' \times 2''$ wounds were generated using a

pressure and temperature controlled metallic die after removal of hair from the selected areas and surgical scrub-preparation (alternating chlorhexidine and alcohol scrub). Wounds were individually covered with Tegaderm (3M) dressing and the entire wound area secured with consecutive bandaging with V.A.C. drape (Owens & Minor), Vetrap, and Elastikon (3M). The bandages were left in place for 3 days, and then removed at day 3 postburn under general anesthesia for bacterial inoculation. A total of 10^8 CFU of *P. aeruginosa* (n = 12 wounds [2 pigs], PA), *S. aureus* (n = 18 wounds [3 pigs], SA), or both bacteria (n = 12 wounds [2 pigs], CO) in 250 μL of PBS (1×) was inoculated into the wounds topically and dispersed across the surface with a sterile spatula. Control wounds (n = 12 wounds [4 pigs], CT) were topically mock inoculated with 1× PBS. The wounds were covered individually after bacterial inoculation and bandaged as described above. Full-thickness, excisional wound biopsies (oriented in the sagittal plane) were removed at days 7, 14, and 35 postbacterial inoculation (PI) and placed in 10% neutral buffered formalin for >72 hours. Normal/nonburned skin (~1 cm) from each side of the wound was included in the biopsy. Skin samples were adhered to wooden tongue depressors to maintain skin shape prior to fixation.

Tissue processing and imaging

Porcine tissues were paraffin embedded, sectioned (5 μm) and stained with hematoxylin and eosin (H&E). The slides were scanned with Aperio Slide Scanner, Scan Scope XT, up to 40× resolution and viewed, analyzed and measured using ImageScope Software (Leica Biosystems, Buffalo Grove, IL).

Histopathology evaluation

A systematic review of histologic lesions between infection groups followed a detailed rubric developed for various skin healing parameters as outlined in Tables 1 and 2, adapted from Meyers et al.[7] Refer to Figure 1 for depictions of the tissue divisions and locations of measurements. Tissue evaluation was undertaken using routine H&E staining. Detailed descriptions of how to identify each of the graded parameters is outside the scope of this article, examples of pertinent lesions are provided in figures.

The percent surface area occupied in each segment by immature granulation tissue or mature fibrosis, necrosis, blood, edema or fibrin, and histiocytic/granulomatous inflammation or mineral was evaluated (Table 1). A minimum of 10% of the lesion was required to be present in the section evaluated to reach a grade 1. Epithelial responses were measured as detailed in Figure 1B. The epithelial gap was measured across the exposed (lacking epithelium) wound surface as the distance between the tips of the migrating epithelium. Polymorphonuclear inflammation was evaluated using the parameters outlined in Table 2.

Statistics

Statistical analysis was performed with GraphPad Prism version 5.0b (GraphPad, La Jolla, CA) and all graphical data is presented as a mean with standard deviation. Comparisons between infection groups were made with two-way ANOVA and Bonferroni posttesting. Significance was set to p-values < 0.05.

RESULTS

Clinically, all pigs remained healthy and asymptomatic for systemic infection during the duration of the study. Key microscopic findings between experimental groups over the course of infection are presented here.

Inflammation

The early inflammatory response in infected wounds is primarily neutrophilic with lesser amounts of macrophages, eosinophils or lymphocytes, and plasma cells. Of the time points evaluated, maximum inflammatory cell infiltration occurred in all infected wounds at day 14 postinoculation (PI). Inflammation remained primarily neutrophilic at day 35 PI, focused at the superficial half of the wound and became increasingly more histiocytic deeper within the wound bed. In each group, neutrophils were largely absent beyond the level of the mid-dermis (follicular units) when measured in comparison to the adjacent, nonburned skin interface.

Neutrophils were present in all wounds at day 7 PI and all other inflammatory cell types (i.e., eosinophils, macrophages, lymphocytes, and plasma cells; Figure 2C) were present in fewer numbers than neutrophils at this time point. The SA and CO groups contained mostly individualized neutrophils within the superficial wound bed with scattered areas of degenerate neutrophils (suppuration) at the wound surface while PA and CT wounds were coated with suppurative inflammation. Neutrophilic inflammation resolved over time in CT wounds with decreasing amounts at days 14 and 35 PI, corresponding to wound healing. Abscess formation was only identified in PA wounds (Figure 3C) at day 14 PI. Neutrophilic inflammation in all infected groups reached maximal infiltration at day 14 PI and coincided with a peak in histiocytic or granulomatous inflammation amongst the evaluated time points (Figure 2). Neutrophilic inflammation in mono-infected groups was minimal by day 35 PI, corresponding to decreasing wound sizes. CO wounds had thick suppurative exudate at day 35 PI (Figure 2).

In all groups, including CT, macrophages and multinucleated giant cells were focused on large clear vacuoles, interpreted as free lipids released in the burning process. Although differences in the amount of macrophages or histiocytes were not appreciated between any of the experimental groups (including CT wounds) qualitative differences between these groups was apparent (Figure 2). Two morphologic subsets were noted: (1) foamy macrophages with cytoplasmic small caliber distinct clear vacuoles (Figure 3A), and (2) macrophages with amphophilic homogenous cytosol and multinucleated giant cells (Figure 3B). The latter phenotype frequently was focused on extracellular mineral, which was also deposited on collagen bundles with minimal associated inflammation (Figure 2B). Mineral was a primarily feature of infected wound groups, versus CT wounds, and more prominent in SA infections. Although macrophage phenotypes described above were not graded separately, there was a trend toward lipid-laden macrophages in PA wounds and multinucleated giant cells predominating in SA wounds. CO wounds contained a mixture of these phenotypes.

Eosinophils were not identified in CT wounds and uniquely present in monospecies infected wounds (i.e., PA and SA wounds). Individualized eosinophils were present within SA wounds at day 35 PI, throughout all depths of the wound bed. Lymphoplasmacytic nodules (Figure 3D) and foci of macrophages or multinucleated giant cells were also infiltrated by eosinophils of day 35 PI SA wounds. In contrast, PA day 7 wounds contained eosinophils primarily clustered at the superficial wound bed adjacent to the reepithelialized edge. Far fewer eosinophils were present within PA wounds at any other time point. Degranulation of these cells was not a feature in any of the wounds.

Lymphoplasmacytic inflammation was most prominent at day 35 PI (Figure 2) in the infected wounds but not a prominent feature of CT wounds. This inflammation was highest in PA wounds compared to any other infected wound at day 35 PI. In all instances the lymphocytes and plasma cells formed discrete nodules but lacked germinal center formation and rarely the center of these lymphoid aggregates contained a sclerotic mass of collagen (Figure 2A).

Dermal healing

CT wounds exhibited prompt infiltration of the wound with granulation tissue, which remodeled to mature collagen concomitant with a decrease of the dermal wound size (contraction) over time. Contracture was taken as the total length of the wound, when measured from the dermis, between the interfaces of normal dermal collagen and wound bed on either side (Figure 1A). Infected wounds retained necrotic tissue and were slower to infiltrate with granulation tissue at days 7 and 14 PI. Wound contracture was larger in all infected wounds compared to CT wounds. CO wounds had elevated amounts of necrotic tissue at all-time points when compared to the other groups

Extracellular fluid is considered a function of dermal healing due the dependence of this feature on the presence of vascular components such as capillaries (blood supply) and lymphatics (drainage). Neovascularization/Vasculogenesis is dependent on a supporting ground structure such as granulation tissue and collagen. Extracellular fluid was most consistently characterized in all wounds by perivascular or dissecting clear spaces with and without a slight pink tincture (i.e., protein). Extracellular fluid accumulations in infection groups remained comparable to CT wounds except for early PA infections. PA wounds at day 7 PI showed large dissecting accumulations of protein rich edema with fibrinous exudate (Figure 4).

Epithelial response

Mono-infected wounds were significantly larger than CT wounds at days 7 and 14 PI (Figure 5). By day 35 PI, CO wounds were the only infection group with significantly delayed wound healing.

Normal skin thickness was measured in histologic section in all pigs in this cohort at the most distant point from the wound and was calculated to range between ~30 and 50 μm which is in accordance with previous reports.[8] SA and PA wounds maintained thicker wound edges over the course of infection when compared to CT and CO wounds (Figure 6). The average thickness across the epithelial tongue reached ~100 μm and 150 μm for SA and PA

infections (2× and 3× normal), respectively, as early as 7 days PI. PA wounds had the thickest epithelium of all the infection groups at days 7 and 14 PI reaching ~200 μm (>4× normal). SA wounds edges were thickest at day 35 PI with the average thickness of the reepithelialized segment calculated to be over 100 μm and the thickest measurement at >350 μm. Reepithelialized segments of CT and CO wounds averaged ~70 μm and between 72 μm and 106 μm, respectively (Figure 5B and C). Reepithelialized sections in mono-infected wounds contained minimal amounts of compact orthokeratotic and parakeratotic hyperkeratosis and moderate to marked rete-peg formation (Figure 6). These features were not considered separately in the evaluation of the tissue.

DISCUSSION

To the best of our knowledge, this is the first detailed evaluation of the histopathology of infected, healing burn wounds in any pig model to date. Differences in wound healing parameters were demonstrated over the course of the chronic infection between different infective bacterial strains. Importantly, as will be discussed below, there are features of these wounds that recapitulate key features of human burn wounds regardless of inciting cause or comorbidities, which have not been previously described in any animal model.[4,9]

Inflammation

No other animal model has been able to recapitulate long-term (>30 days) wound inflammation without significant host-comorbidity (i.e., diabetes) making this animal model an excellent system by which to study long-term effects of chronic neutrophilic inflammation on wound healing.[2,10,11]

While macrophage quantities were not discernably different amongst the different experimental groups, cells exhibited differing phenotypes dependent on infective bacterial species. The significance of this observation is not clear. We speculate that the predominance of vacuolated macrophages in PA wounds and mineral associated and multinucleated giant cells in SA wounds may correlate to an altered activation state or physiologic demand as *in vitro* manipulation of macrophage activation states alters cell morphologies.[12,13]

The increased numbers of eosinophils in mono-species infected wounds, early in PA infected wounds and late in SA infected wounds, is peculiar. Evidence of these cell types being identified in human chronic wounds is lacking but the importance of this cell type in wound healing and in the recovery from *S. aureus* and *P. aeruginosa* infection has been documented.[14–17] Further studies are needed to understand the significance of these findings.

Dermal healing

As wounds heal, the removal of necrotic tissue is a pivotal event to aide in the clearance of inflammatory cytokines, nidi for bacterial infection, granulation tissue formation and epithelial migration. Retention of necrotic tissue is associated with delayed wound healing and chronic wound formation.[18] Since there is standardization of the initial amount of necrotic tissue inflicted in this animal model, increased amounts are proposed to be retained via the following mechanisms: altered immune cell responses (i.e., phagocytosis), delayed neovascularization (i.e., delivery of inflammatory cells, nutrients, and oxygen) or lack of

appropriate microenvironment for fibroblast maturity and differentiation. In this study, CO wounds, compared with mono-infected or CT wounds displayed a greater amount of retained necrotic tissue and stromal immaturity and this may have contributed to delayed reepithelialization.

The bacteria used here are specifically able to alter stromal components and inflammatory cells and their responses. Human stromal cells are susceptible to soluble factors of both *S. aureus* and *P. aeruginosa* biofilms, decreasing cell differentiation, viability, migration and angio-genesis.[19] The inhibition of stromal cells is anticipated to affect wound-healing parameters such as is present in this study (i.e., contraction, necrotic tissue accumulation, hemorrhage, and edema). It is clear by the total dermal wound size in each of the infection groups that the microenvironment did not allow for the same degree of contracture as seen in control wounds.[20,21] Further study is required in this area but this model may prove to be physiologically relevant to human chronic wounds and therefore increase the ability to study this unique microenvironment.[22]

Epithelial response

One of the key parameters defining chronic human wounds is a hyper-proliferative wound edge with hyperkeratosis.[4] This feature is rarely reported in current chronic skin wound animal models with more emphasis placed on reepithelialization. Reepithelialized sections of the wounds in this study displayed minimal amounts of compact hyperkeratosis, which was not equivocal to human chronic wound descriptions.[4] Using mono-infections with either SA or PA, the reepithelialized wound edge reached 2–3× or nearly up to 4× normal skin thickness, respectively, within 7 days PI and this was maintained until at least day 14 PI. At no point in the course of healing did CT wounds average a thickness above 2× normal. Therefore, it appears that SA and PA have a dramatic effect on keratinocyte proliferation rates as well as an impedance to the migration of the keratinocytes as evidenced by delayed wound closure in the mono-infected groups at day 7 and 14 PI. Given our previous use of this model and determination of biofilm mode of growth of PA in that model we speculate that this response may be due to the specific biofilm mode of growth of these bacterial species.[6]

Extracellular products from biofilms of *S. aureus* and *P. aeruginosa* have a significant effect on epithelial proliferation and migration *in vitro*.[23] It is speculated that a similar mechanism may be produced in these porcine infections. Marano et al. identified that human epidermal keratinocytes were highly susceptible to cytolytic properties of the conditioned biofilm media of both bacterial species while at reduced concentrations there was inhibition of migration and proliferation.[23] Others have identified *S. aureus* and *P. aeruginosa* specific factors that may enhance epithelial proliferation.[24,25] Therefore, the effects seen here may not be specific to a bacterial mode of growth.

Surprisingly, the hyperproliferative wound edge was not present in CO wounds. This may be a dose dependent phenomena, however, we consider this less likely given that the delay in reepithelialization was of a similar magnitude at days 7 and 14 PI and even more pronounced at day 35 PI when compared to mono-infected wounds. Therefore, the effect of

both of these bacteria together appears to produce reduced epithelial proliferation and migration.

The detailed evaluation of these wounds has shown great similarity to key features of the chronic human wounds, regardless of inciting cause. Importantly, the effects of bacterial infection on host responses were widespread (i.e., epidermal, dermal, and inflammatory) and when conducting animal experiments for evaluation of treatment modalities and bacterial effects all parameters should be evaluated. The information gained from these studies will aide in evaluating the effect of interventions for both bacterial and host responses.

ACKNOWLEDGMENTS

All animal work would not be possible without the aide and expertise of Jennifer Dickerson. The authors acknowledge the skill and aid in figure preparation by Thomas Heban.

Source of Funding: The Comparative Pathology & Mouse Phenotyping Shared Resource of The Ohio State University, which is supported in part through an NCI Cancer Center Support Grant P30 CA016058, performed Immunohistochemisty. Public Health Services grants NR013898 and AI097511 (DJW) supported this work.

REFERENCES

1. Lindholm C, Searle R. Wound management for the 21st century: combining effectiveness and efficiency. Int Wound J 2016; 13(Suppl.2): 5–15.
2. Ganesh K, Sinha M, Mathew-Steiner SS, Das A, Roy S, Sen CK. Chronic wound biofilm model. Adv Wound Care (New Rochelle) 2015; 4: 382–8. [PubMed: 26155380]
3. Rhoads DD, Cox SB, Rees EJ, Sun Y, Wolcott RD. Clinical identification of bacteria in human chronic wound infections: culturing vs. 16S ribosomal DNA sequencing. BMC Infect Dis 2012; 12: 321 [PubMed: 23176603]
4. Golinko MS, Joffe R, de Vinck D, Chandrasekaran E, Stojadinovic O, Barrientos S, et al. Surgical pathology to describe the clinical margin of debridement of chronic wounds using a wound electronic medical record. J Am Coll Surg 2009; 209: 254–60.e1. [PubMed: 19632603]
5. Stover CK, Pham XQ, Erwin AL, Mizoguchi SD, Warrener P, Hickey MJ, et al. Complete genome sequence of Pseudomonas aeruginosa PAO1, an opportunistic pathogen. Nature 2000; 406: 959–64. [PubMed: 10984043]
6. Roy S, Elgharably H, Sinha M, Ganesh K, Chaney S, Mann E, et al. Mixed-species biofilm compromises wound healing by disrupting epidermal barrier function. J Pathol 2014; 233: 331–43. [PubMed: 24771509]
7. Myers AH, Postlethwait RW, Smith AG. Histologic grading of the experimental healing wound. Arch Surg 1961; 83: 771–4.
8. Summerfield A, Meurens F, Ricklin ME. The immunology of the porcine skin and its value as a model for human skin. Mol Immunol 2014; 66: 14–21. [PubMed: 25466611]
9. Pastar I, Stojadinovic O, Yin NC, Ramirez H, Nusbaum AG, Sawaya A, et al. Epithelialization in wound healing: a comprehensive review. Adv Wound Care (New Rochelle) 2014; 3: 445–64. [PubMed: 25032064]
10. Metcalf D, Bowler P, Parsons D. Wound biofilm and therapeutic strategies In: Dhanasekaran D, Thajuddin N, editors. Microbial biofilms-importance and applications. Rijeka: InTech, 2016: 271–98.
11. Nunan R, Harding KG, Martin P. Clinical challenges of chronic wounds: searching for an optimal animal model to recapitulate their complexity. Dis Model Mech 2014; 7: 1205–13. [PubMed: 25359790]
12. Gordon S Alternative activation of macrophages. Nat Rev Immunol 2003; 3: 23–35. [PubMed: 12511873]

13. McWhorter FY, Wang T, Nguyen P, Chung T, Liu WF. Modulation of macrophage phenotype by cell shape. Proc Natl Acad Sci USA 2013; 110: 17253–8. [PubMed: 24101477]
14. Lee JJ, Jacobsen EA, McGarry MP, Schleimer RP, Lee NA. Eosinophils in health and disease: the LIAR hypothesis. Clin Exp Allergy 2010; 40: 563–75. [PubMed: 20447076]
15. Rodriguez-Fernandez A, Andaluz-Ojeda D, Almansa R, Justel M, Eiros JM, Ortiz de Lejarazu R. Eosinophil as a protective cell in *S aureus*. ventilator-associated pneumonia. Mediators Inflamm 2013; 152943. [PubMed: 24082429]
16. Linch SN, Kelly AM, Danielson ET, Pero R, Lee JJ, Gold JA. Mouse eosinophils possess potent antibacterial properties *in vivo*. Infect Immun 2009; 77: 4976–82. [PubMed: 19703974]
17. Song BZ, Donoff RB, Tsuji T, Todd R, Gallagher GT, Wong DT. Identification of rabbit eosinophils and heterophils in cutaneous healing wounds. Histochem J 1993; 25: 762–71. [PubMed: 7506704]
18. Schultz GS, Sibbald RG, Falanga V, Ayello EA, Dowsett C, Harding K, et al. Wound bed preparation: a systematic approach to wound management. Wound Repair Regen 2003; 11 (Suppl. 1): S1–28. [PubMed: 12654015]
19. Ward CL, Sanchez CJ, Jr, Pollot BE, Romano DR, Hardy SK, Becerra SC, et al. Soluble factors from biofilms of wound pathogens modulate human bone marrow-derived stromal cell differentiation, migration, angiogenesis, and cytokine secretion. BMC Microbiol 2015; 15: 75. [PubMed: 25886581]
20. Rose LF, Chan RK. The burn wound microenvironment. Adv Wound Care (New Rochelle) 2016; 5: 106–18. [PubMed: 26989577]
21. Darby IA, Laverdet B, Bonté F, Desmoulière A. Fibroblasts and myofibroblasts in wound healing. Clin Cosmet Investig Dermatol 2014; 7: 301–11.
22. Tiwari VK. Burn wound: how it differs from other wounds? Indian J Plast Surg 2012; 45: 364–73. [PubMed: 23162236]
23. Marano JR, Wallace JH, Wijeratne D, Fear WM, Wong SH, O'Handley R. Secreted biofilm factors adversely affect cellular wound healing responses in vitro. Sci Rep 2015; 5: 13296. [PubMed: 26278131]
24. Preciado D, Caicedo E, Jhanjee R, Silver R, Harris G, Juhn SK, et al. *Pseudomonas aeruginosa* lipopolysaccharide induction of keratinocyte proliferation, NF-kappa B, and cyclin D1 is inhibited by indomethacin. J Immunol 2005; 174: 2964–73. [PubMed: 15728509]
25. Haugwitz U, Bobkiewicz W, Han SR, Beckmann E, Veerachato G, Shaid S, et al. Pore-forming *Staphylococcus aureus* alpha-toxin triggers epidermal growth factor receptor-dependent proliferation. Cell Microbiol 2006; 8: 1591–600. [PubMed: 16984414]

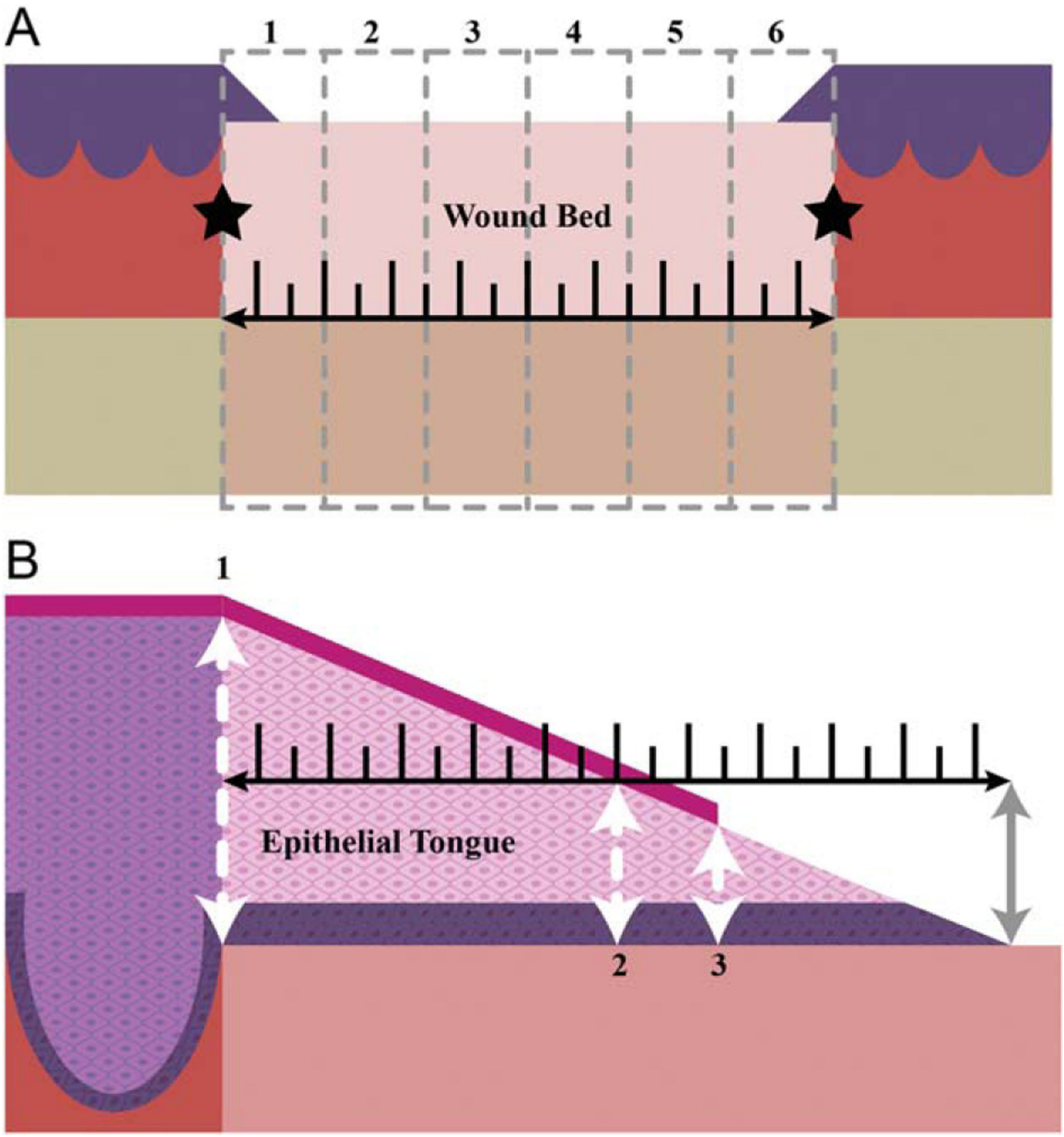

Figure 1.

Tissue divisions for microscopic evaluation. (A) The total wound bed length (black ruler) was divided into six equidistant segments (oriented superficial to deep, grey dashed lines). The bounds of the wound bed are defined by the interface of normal dermal collagen and thermally injured tissue (black stars). Each segment (1–6) was evaluated using the scheme in Tables 1 and 2. The scores from each segment were averaged for a final wound score, per parameter.(B) The epithelium covering the wound bed (epithelial tongue) was measured from the base (far left white arrow, #1) to the tip (gray arrow). Epithelial thicknesses were measured at 3 points from each side of the wound: #1) base (far left white arrow) #2) mid-point (middle white arrow) #3) epithelial tip (far right white arrow). Measurements were taken in areas in which there was a discrete stratum corneum formed (magenta line) but

thickness measurements only included the stratum basale (dark purple) and stratum spinosum (light pink) [Color figure can be viewed at wileyonlinelibrary.com]

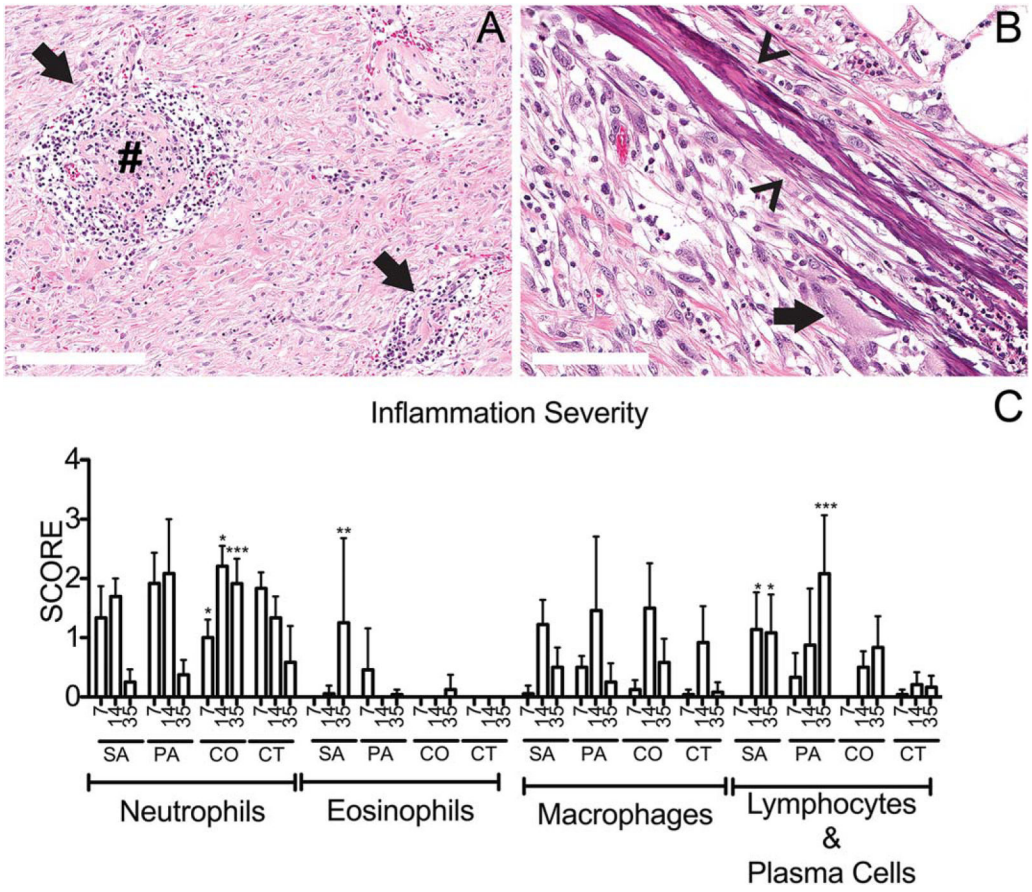

Figure 2.

Scoring inflammation in the infected chronic wound. (A) *P. aeruginosa* infected wounds at 35 days postinfection (PI) contained organized lymphoplasmacytic nodules (arrows) within the dermal wound bed. Occasionally these nodules contained a central core of dense hylanized collagen (#). (B) *S. aureus* infected wounds contained collagen bundles with mineral deposition (arrowheads) with minimal amounts of associated inflammation (multinucleated giant cell, arrow) at day 14 PI. (C) Using the grading scheme outlined Table 1, the individual wound histology parameters were scored and averaged from six segments evenly distributed across the wound. Inflammatory parameters were scored 0–4 as outlined in Tables 1 and 2. For the graph above, C: *x*-axis represents time points day 7, 14, and 35 postinfection; SA, *S. aureus*, PA, *P. aeruginosa*, CO, coinfected wounds, and CT, control wounds. The mean scores are graphed here with standard deviation error bars and statistical significance measured by 2-way ANOVA, $p < 0.05$ [Color figure can be viewed at wileyonlinelibrary.com]

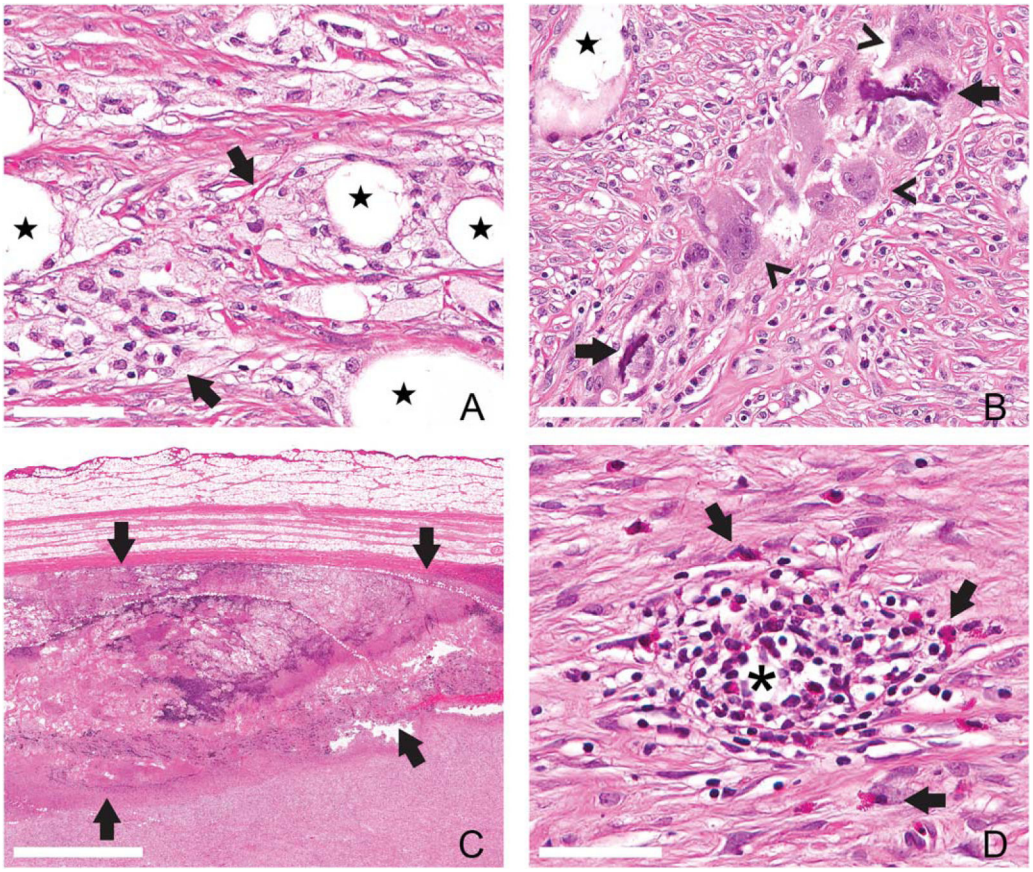

Figure 3.

Inflammation of the infected chronic wound. Granulomatous and histiocytic inflammation did not vary in quantity over the course of infection but tended to accumulate around large clear vacuoles (free lipid, star, A and B, scale bar = 60 μm). *P. aeruginosa* infected wounds (PA) at day 14 postinfection (PI) contained foamy macrophages with small, discrete clear vacuoles filling the cell cytoplasm (arrows, A). Granulomatous inflammation of *S. aureus* infected wounds (SA) at day 14 PI centered on extracellular mineral (arrows, B, scale bar = 80 μm) with multinucleated giant cells (arrowheads, B). Abscesses only formed in PA wounds at day 14 PI (bounded by arrows, 2C, scale bar = 2 mm). Eosinophils were present as individualized scattered cells in SA wounds at day 35 PI (clear arrows, D, scale bar = 50 μm) or within organized lymphoplasmacytic nodules (*) [Color figure can be viewed at wileyonlinelibrary.com]

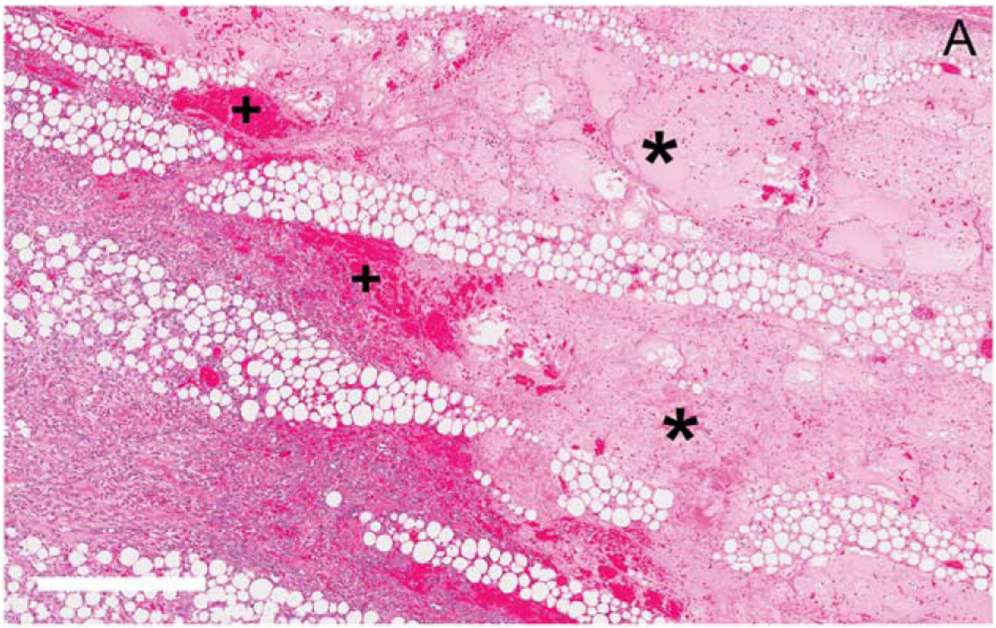

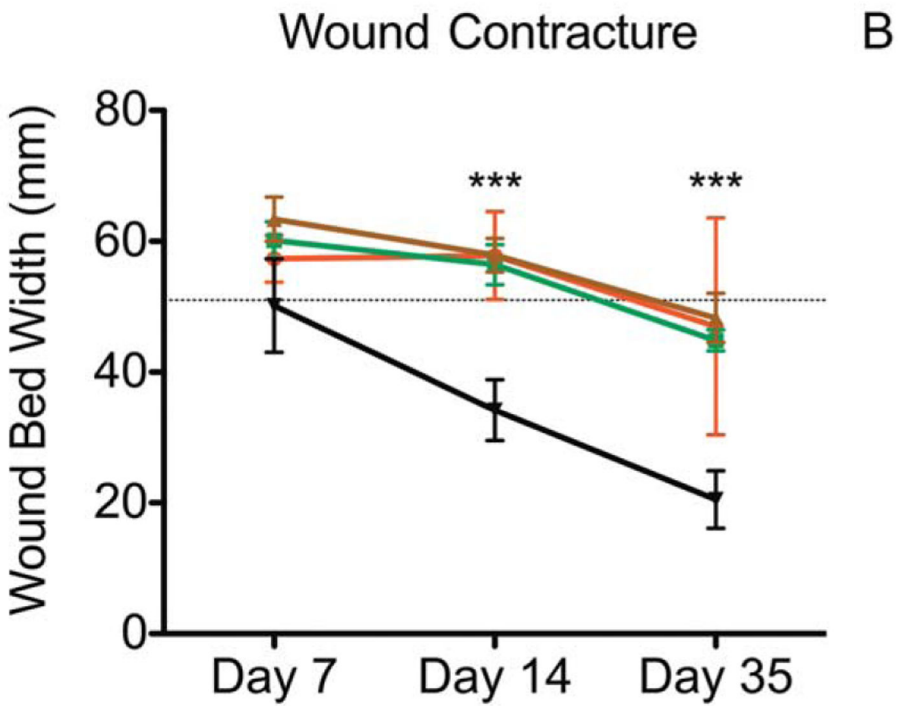

Figure 4.

Dermal responses to infection in chronic wounds.(A) *P. aeruginosa* infected wounds at day 7 postinoculation (PA) contained marked amounts of proteinaceous edema (*) filling necrotic areas and cuffed by moderate amounts of hemorrhage (+). (B) Infection, regardless of bacterial strain (red = *S. aureus*–infected, green = PA, brown = coinfected), delayed the contraction of the dermal wound bed compared to control wounds (black line). Graphed are mean measurements with standard deviation, statistical significance is considered at $p < 0.05$

using 2-way ANOVA. *x*-axis represents time points day 7, 14, and 35 postinfection [Color figure can be viewed at wileyonlinelibrary.com]

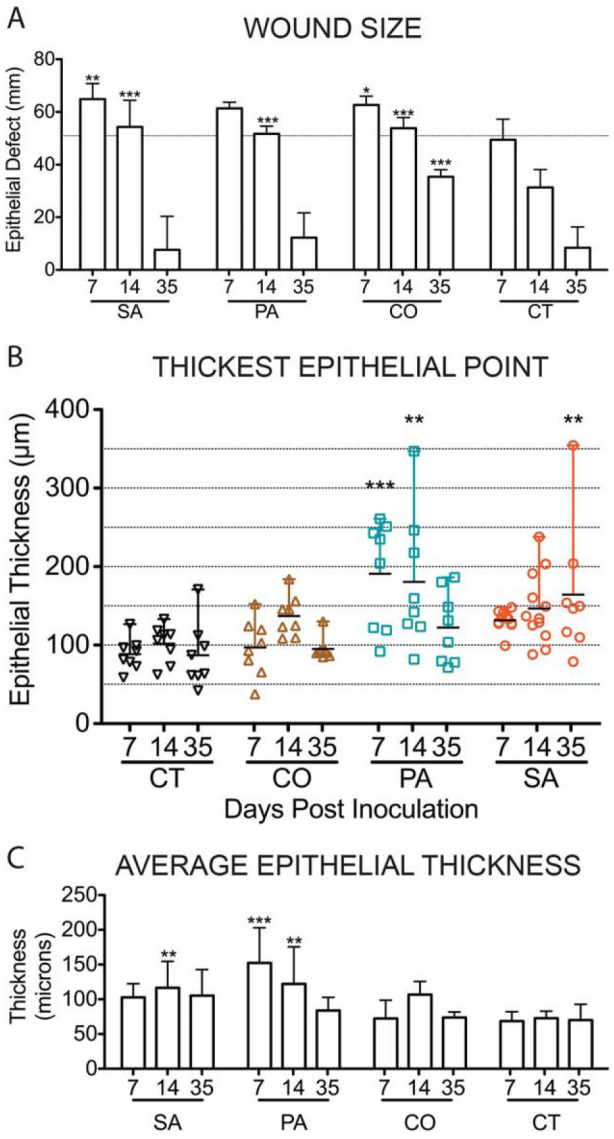

Figure 5.

Scoring epidermal responses to infection in chronic wounds. Using the epithelial measurements detailed in Figure 1 and Table 1, epithelial responses were analyzed by determining the wound size/epithelial defect with the size of the burning instrument indicated by the horizontal dashed line (A), the thickest point measured out of the 3 described in Figure 1 within the new epithelial tongues (B) and the average thickness across the epithelial tongue as measured by 3 separate, defined points (C). For all the graphs above: *x*-axis represents time points day 7, 14, and 35 postinfection; SA, *S. aureus*, PA, *P. aeruginosa*, CO, coinfected wounds, and CT, control wounds. The mean scores are graphed here with standard deviation error bars and statistical significance measured by 2-way ANOVA, $p < 0.05$ [Color figure can be viewed at wileyonlinelibrary.com]

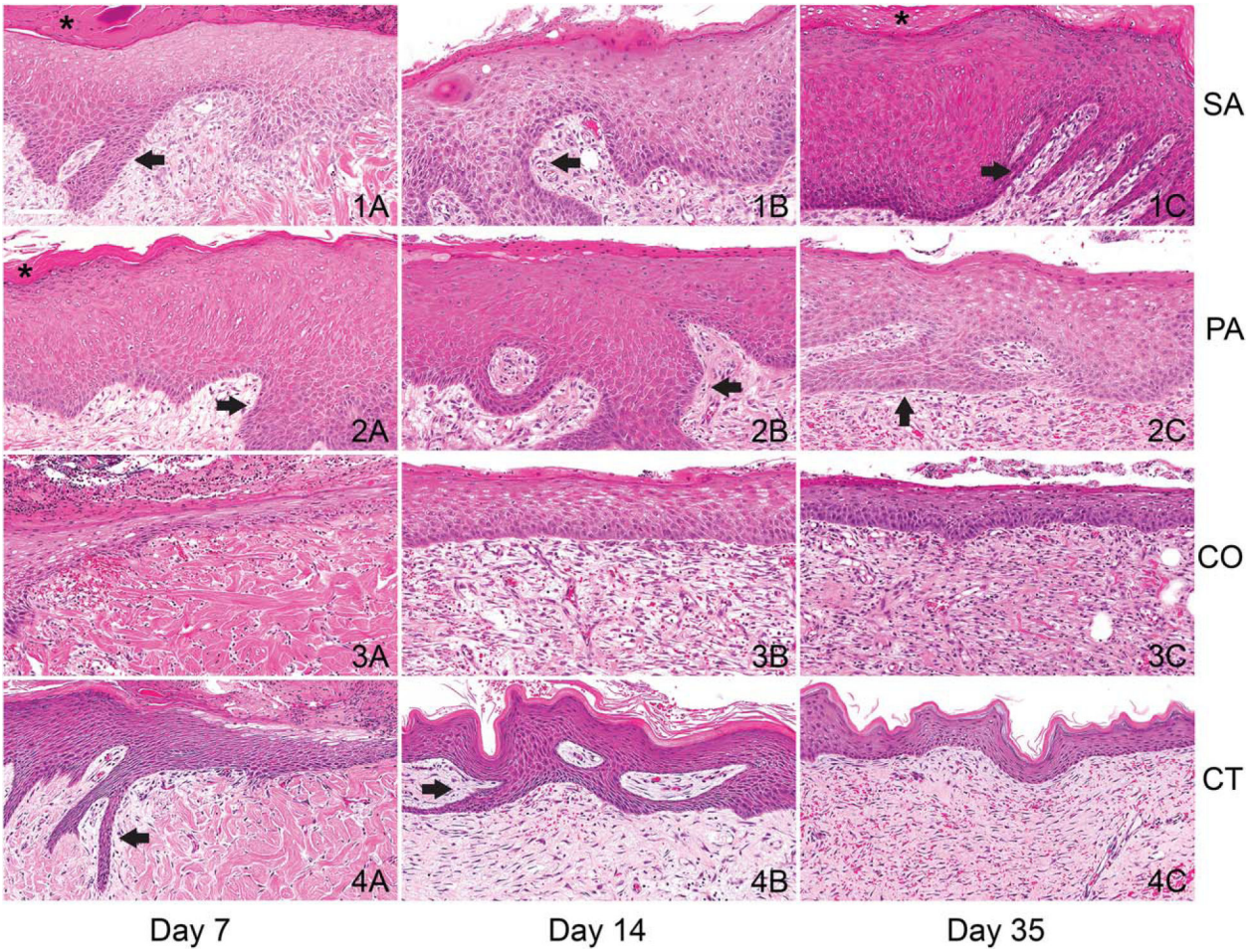

Figure 6.

Epithelial responses to infection in chronic wounds. The reepithelialized section of skin (wound edge) covering mono-infected wounds, *S. aureus* (SA) and *P. aeruginosa* (PA) infected wounds (rows 1 and 2), were hyper-proliferative compared to coinfected and control wounds (CO, row 3 and CT row 4, respectively) at all time points (columns 1, 2, 3 are days 7, 14, and 35 postinfection (PI), respectively). Proliferation was accompanied by rete-peg formation (arrows) and mild hyperkeratosis (*). Scale bars = 100 μm [Color figure can be viewed at wileyonlinelibrary.com]

Table 1.

Microscopic evaluation scheme of healing burn wounds

	Grade 0	Grade 1	Grade 2	Grade 3	Grade 4
Inflammation					
Neutrophils *		Mild	Moderate	Marked	Severe
Eosinophils *		Mild	Moderate	Marked	Severe
Lymphocytes & plasma cells	0 to 5 Organized Units	6 to 10	11 to 15	16 to 20	>21
Histiocytes/MNGC †/mineral	<10%	10 to 25%	up to 50%	up to 75%	>80%
Dermal Response					
Blood/edema	<10%	10 to 25%	up to 50%	up to 75%	>80%
Necrosis, stromal	<10%	10 to 25%	up to 50%	up to 75%	>80%
Granulation tissue	<10%	10 to 25%	up to 50%	up to 75%	>80%
	Characterized by fibroblasts and increased density of small caliber capillaries				
Mature dermis	<10%	10 to 25%	up to 50%	up to 75%	>80%
	Characterized by mature, dense collagen and fibrocytes				
Dermal wound bed	Measure Length				
Epithelial Response					
Epithelial proliferation	>3× or healed wound	2.5×	2×	1.5×	≤Normal thickness
Epithelial gap	<40% Open	Up to 40%	Up to 60%	Up to 80%	>100%

* Details provided in Table 2.

† Multinucleated giant cells.

Table 2.

Microscopic evaluation scheme of acute inflammation

Neutrophil Severity	
Grade 0	Scattered individual cells may be present in the wound but primarily intravascular/margin-ating or widely spaced within the wound
Grade 1	Viable/nondegenerate neutrophils as individual cells within the wound. If suppuration is present it does not coat the surface or span the length of the segment being graded
Grade 2	Variably thick suppurative inflammation that spans the length of the segment
Grade 3	Dense consistent thickness of suppurative inflammation that spans the length of the segment and neutrophils present within the wound bed below are in small clusters or individual
Grade 4	Large pools of suppurative exudate over the length of the segment with large numbers present in the underlying wound bed, mostly present in clusters. Abscess formation.
Eosinophil Severity	Scored based on the number of foci of clustered eosinophils or numerous individual cells, when viewed at 10×.
Grade 0	Less than 10 foci
Grade 1	11–20 foci
Grade 2	21 to 30 foci
Grade 3	31 to 40 foci
Grade 4	>40 foci